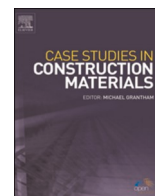




ELSEVIER

Contents lists available at ScienceDirect

Case Studies in Construction Materials

journal homepage: www.elsevier.com/locate/cscm

Effects of concrete/gypsum bedding layers and their inclination angles on the tensile failure mechanism: Experimental and numerical studies

Soheil Abharian^a, Vahab Sarfarazi^{b,*}, Haleh Rasekh^c, Masoud Behzadinasab^d

^a Department of Mining and Metallurgical Engineering, Amirkabir University, Tehran, the Islamic Republic of Iran

^b Department of Mining Engineering, Hamedan University of Technology, Hamedan, the Islamic Republic of Iran

^c School of Civil and Environmental Engineering, University of Technology Sydney, Sydney, Australia

^d School of Engineering, Brown University, Providence, USA

ARTICLE INFO

Keywords:

Bedding layer

Gypsum

Concrete

Tensile crack

And three-point bending

ABSTRACT

This paper investigates the influence of concrete/gypsum bedding layers and their orientation angles on the tensile failure mechanism in the three-point bending test based on experiments and numerical simulations. Rectangular samples containing different combinations of concrete and gypsum layers were prepared, i.e. one layer of gypsum and one layer of concrete, one layer of gypsum and two layers of concrete, and two layers of gypsum and two layers of concrete. In each configuration, bedding layer angles varied between 0° and 90° with increment of 30°. A total of 36 specimens including 12 configurations were prepared and tested. In addition, numerical simulations were conducted on the concrete/gypsum bedding layers at different angles of 0°, 15°, 30°, 45°, 60°, 75°, and 90°. Results show that the bedding layer orientation and bedding layer thickness affect the observed tensile failure process including the failure pattern and tensile strength. A pure tensile failure occurred when the bedding layer angle was 0°, while a sliding failure evolved by increasing the joint angle. When the bedding layer angle was 90°, the failure in boundary of layer was observed. Specimens with one layer of concrete and one layer of gypsum at 0° inclination angle had the highest tensile strength. However, increasing the number of layers and inclination angles decreased the tensile strength of specimens as the number of weak layers in the direction of loading increased.

1. Introduction

The cleavage, foliation, schistosity, joints, micro-and macro-fissures, and bedding plane play a significant role in the anisotropy characteristic of the rock [3]. However, the common isotropic and anisotropic sedimentary rocks depend on the bedding planes or spacing, or restriction of the growth during deposition. Metamorphic rocks are primarily anisotropic because of the consequences of both schistosity and cleavage [62,63]. Magmatic rocks, like granite, might have anisotropy features because of the micro-cracks under tectonic plate movement, and understanding the characteristics of the magmatic rocks are vital for many rock engineering projects [20–22,54]. Such features have been investigated via uniaxial compressive strength (UCS) and triaxial loading condition tests on sedimentary rocks [4,12,16,23,48]; sandstones [36,61], and [3]; phyllites [60]; artificial materials [78,79], and [81]; gneisses and

* Corresponding author.

E-mail address: vahab.sarfarazi@gmail.com (V. Sarfarazi).

<https://doi.org/10.1016/j.cscm.2022.e01272>

Received 11 May 2022; Received in revised form 7 June 2022; Accepted 25 June 2022

Available online 30 June 2022

2214-5095/© 2022 The Author(s). Published by Elsevier Ltd. This is an open access article under the CC BY license (<http://creativecommons.org/licenses/by/4.0/>).

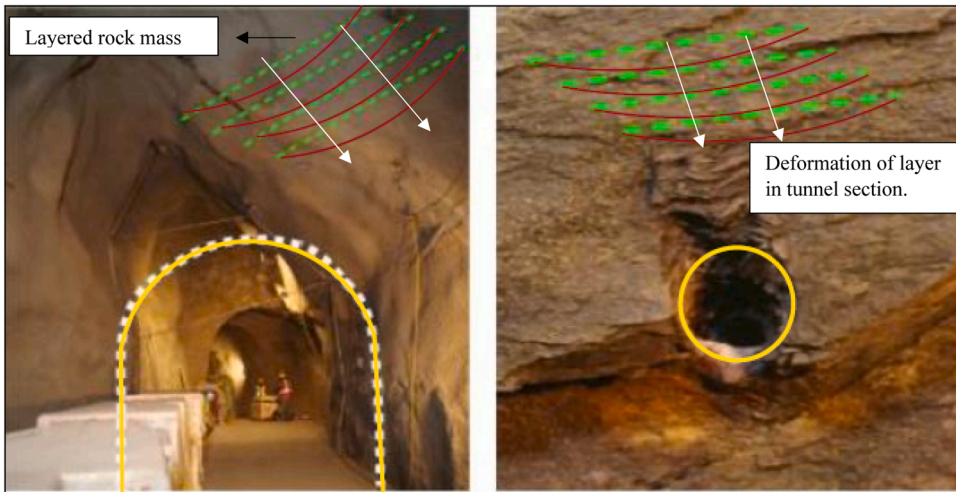


Fig. 1. The possible deformation of underground tunnel with crack patterns by Li [47].



Fig. 2. Pillar that had an original width-to-height ratio of 1.7 failed by progressive spelling [28].

Table 1
Concrete mix design used in this study.

Gravel (g)	Sand (g)	Cement (g)	Water (cc)	Superplasticizer (g)	Micro silica (g)
3000	10,500	2800	1500	120	90

Table 2
Characteristics of cement and Silica fume.

Properties	Cement	Silica fume
Physical properties		
Specific gravity (gr/cm ³)	3.15	2.20
Surface area (m ² /kg)	320	20,000
Size (micron)	–	0.1
Bulk density (kg/m)	–	576
Initial setting time (min)	45	–
Final setting time (min)	375	–
Chemical properties (%)		
SiO ₂	90–96	20–25
Al ₂ O ₃	0.5–0.8	4–8

Table 3
Physical properties of sand.

Index	value
Specific gravity (gr/cm^3)	2.63
Passing 4.75-mm sieve (%)	100
Maximum dry density (kN/m^3)	15.5
Minimum dry density (kN/m^3)	12.3
D_{10}	0.194
D_{50}	0.322
D_{60}	0.344

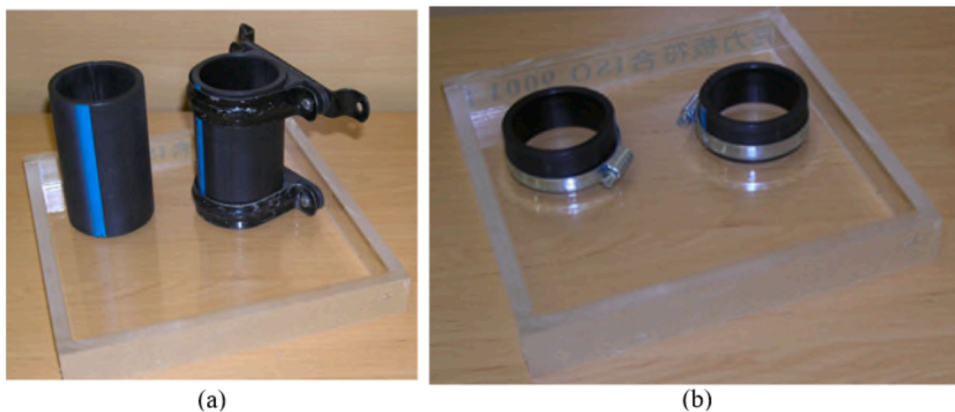


Fig. 3. (a) Cylindrical mold with 54 mm in diameter and 112 mm in length, (b) disc mold with 54 mm in diameter and 27 mm in thickness.



Fig. 4. a) Brazilian test machine, b) uniaxial test machine.

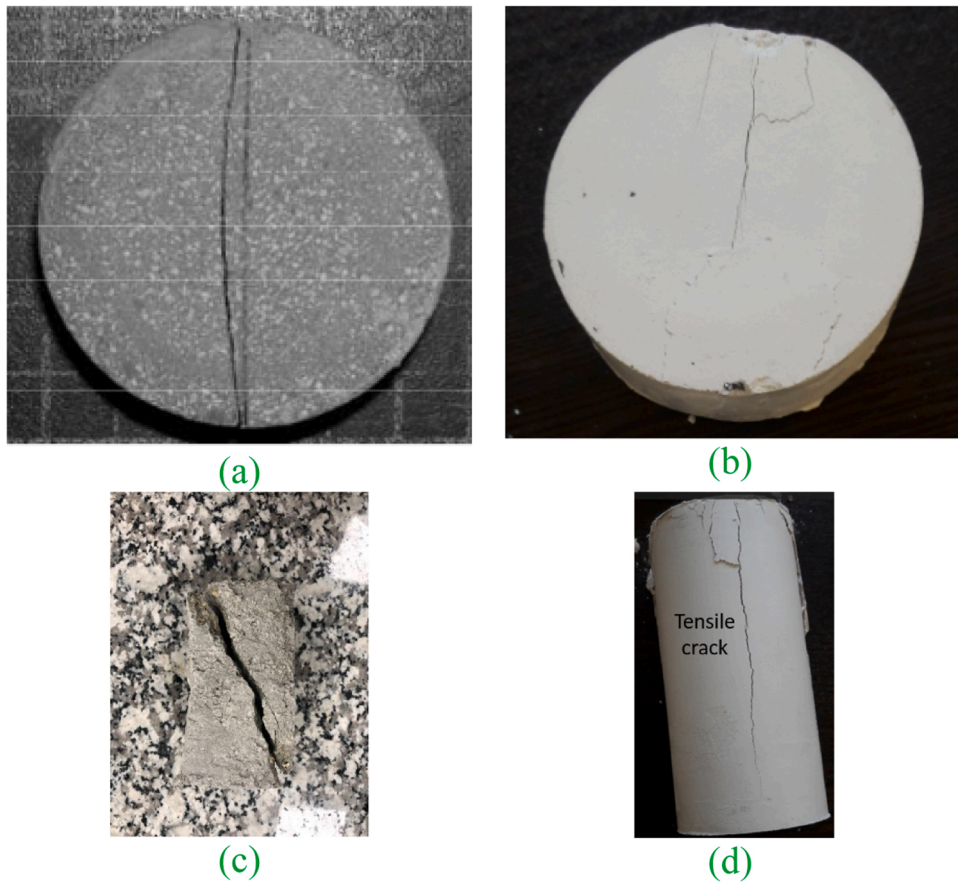


Fig. 5. Crack growth in (a) concrete specimen, and (b) gypsum specimen subjected to Brazilian tensile strength test, and crack growth in (c) concrete specimen, and (d) gypsum specimen subjected to UCS test.

Table 4

The schematic view of gypsum-concrete interface layers; (a) one layer of gypsum and one layer of concrete, (b) one layer of gypsum and two layers of concrete, and (c) two layers of gypsum and two layers of concrete inclined at different angles (0°, 30°, 60° and 90°).

Inclination angle (°)				
0	30	60	90	
				a
				b
				c

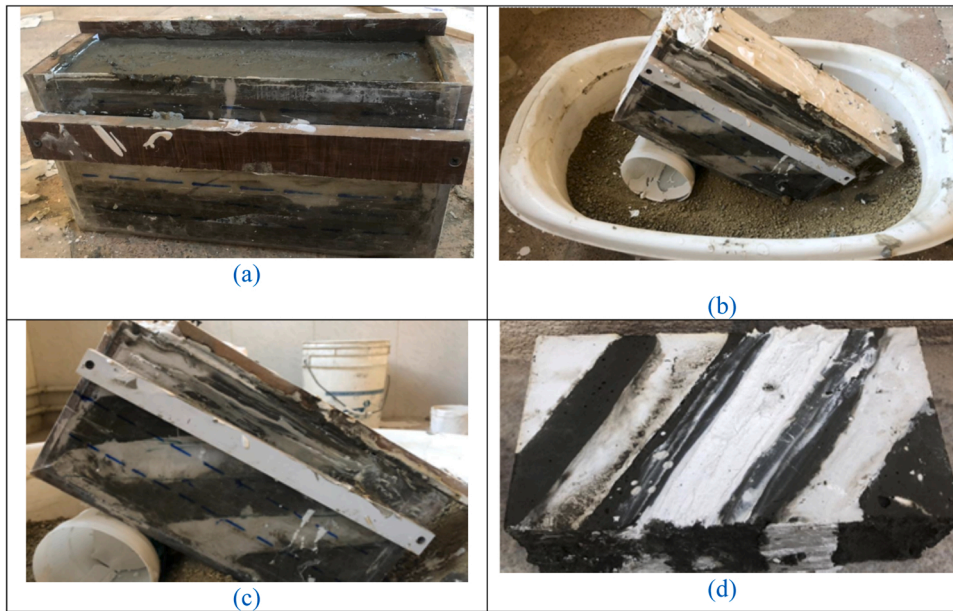
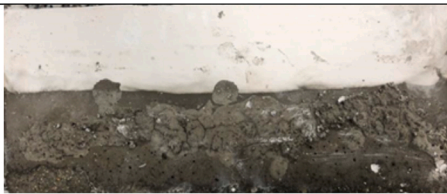







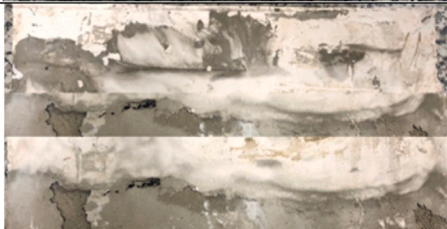





Fig. 6. (a) Plexiglas mold, (b) a rolling cylinder moves below the mold for the creation of layers at specific angles, (c) cap on the mold surface, and (d) prepared gypsum and concrete layers.

schists [9,24,52,53,64], and [67]; mudrocks [2]; quartz mica schist [99]; and travertine [93]. Anisotropy of sample under UCS test value is linked to the fabric of micro-cracks in magmatic rocks [17]. Mechanical and anisotropic features of concrete and rocks have been widely investigated by several researchers via leading lab examinations [8,13,37,42,44,45,69] and numerical modellings [45,47,70,72–74,95]. Changing the shape of crack [38,75] and crack growth are normally examined to address the anisotropic properties [76,82,90]. The effects of rock anisotropy on the tensile strength of rock via the Brazilian test were investigated by Hobbs [35] on siltstone, sandstone and mudstone; McLamore and Gray [48] on shale; Tavallali and Vervoort [80] and Chen et al. [14] on sandstone; Debecker and Vervoort [19] on slate; and [21,22] and Dai and Xia [20] on granite. The outcomes demonstrate that the tensile strength and crack growth phenomena depend on the orientation of the weakness planes, and two or three different failure modes were recognized in the same experiments. Chen et al. [14] introduced two significant modes of tensile splitting; parallel to the loading direction of sample and by shear failure along the sample layers. In addition, the results of studies by Dai and Xia (2013) and [21,22] indicated that the pre-existing micro-cracks affect the tensile strength anisotropy. Usage of the point load test for evaluating the strength of the isotropic and anisotropic rocks is widespread [7,10,11,41,42,77]. However, the angle between the loading direction and foliation planes plays a critical role in the point load index of anisotropic rocks. The specimen has minimum tensile strength when loading direction was parallel to foliation plane. Furthermore, Basu and Kamran [7] demonstrated that the UCS value of anisotropic rock could be predictable from the point load test. The crack growth of the tested samples showed an identical pattern. Concrete is considerably more delicate below tensile load rather than other types of loading. Brazilian tests on concrete have been widely conducted to determine the tensile behaviors of concrete materials [25,26,39,84–86,88,91,96,97]. The effects of temperature, confining pressure, strain rate, water content, and chemical properties on the tensile strength of specimens have been studied previously; however, the attention to heterogeneity was absent [5,6,30,32,33,49,51,83,94,98]. Therefore, evaluating the tensile strength of concrete with discontinuities is vital. The review of previous studies highlights the significant attention to the crack features of anisotropic samples [18,50]; Dai and Xia, 2013; [34,43]. Nevertheless, very limited studies have examined the effects of rock notch on the rock strength [29]. It has been known for a long time that the expanding amount of joints could noticeably reduce the concrete strength [52,55,78,87]. However, the strength of the bi-material bedding layer and the relationship with orientations on the tensile strength of the concrete was absence. The tensile behaviors of layered rocks have been extensively investigated; however, outcomes of layered samples under different loading conditions have been rarely reported. The fracturing pattern for an underground tunnel with existing natural flaws was investigated by Li [47] as shown in Fig. 1. In the in-situ survey site, mainly tensile failures were recorded. An anisotropic solid reaction from an underground tunnel section was calculated with a moderate convergence rate by Lisjak et al. [46]. The movements in the Y-axis to the X-axis (layers orientations) were comparatively four times larger than displacements parallel to the layers. The convergence in the layered Lias limestone in the Löttschberg underground excavation was investigated by Seingre [66]. The orientation of discontinuities greatly influenced the steel sets and surrounding rock masses. The anisotropy displacements observed in underground excavation case studies are mainly perpendicular to the joints and layered orientations, which perfectly agrees with numerical simulations [89,92]. Layers in large massive slabs, beams-walls, pillars-walls and voluminous constructions can be deflected and leads to drastic failure (Fig. 2). In this context, many design structures in mining practice require detailed rock mechanics analyses using accurate data and advanced numerical tools. Stress and stability analyses, indeed, can be carried out using continuous and/or discontinuous numerical approaches, and they are currently used in the civil and mining engineering sectors due to the possibility to take account of complex

Table 5

Prepared gypsum-concrete specimens including; (a) one layer of gypsum and one layer of concrete, (b) one layer of gypsum and two layers of concrete, and (c) two layers of gypsum and two layers of concrete inclined at different angles (0°, 30°, 60° and 90°).

Angle (°)		Angle (°)		
0		30		
60		90		a
0		30		
60		90		b
0		30		
60		90		c

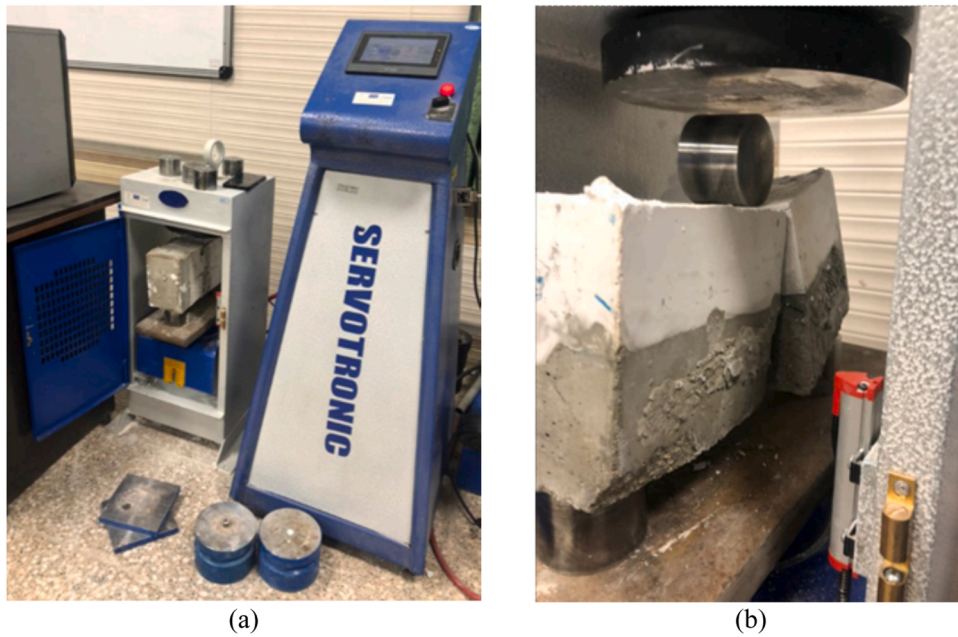


Fig. 7. Specimens are subjected to the three point bending test.

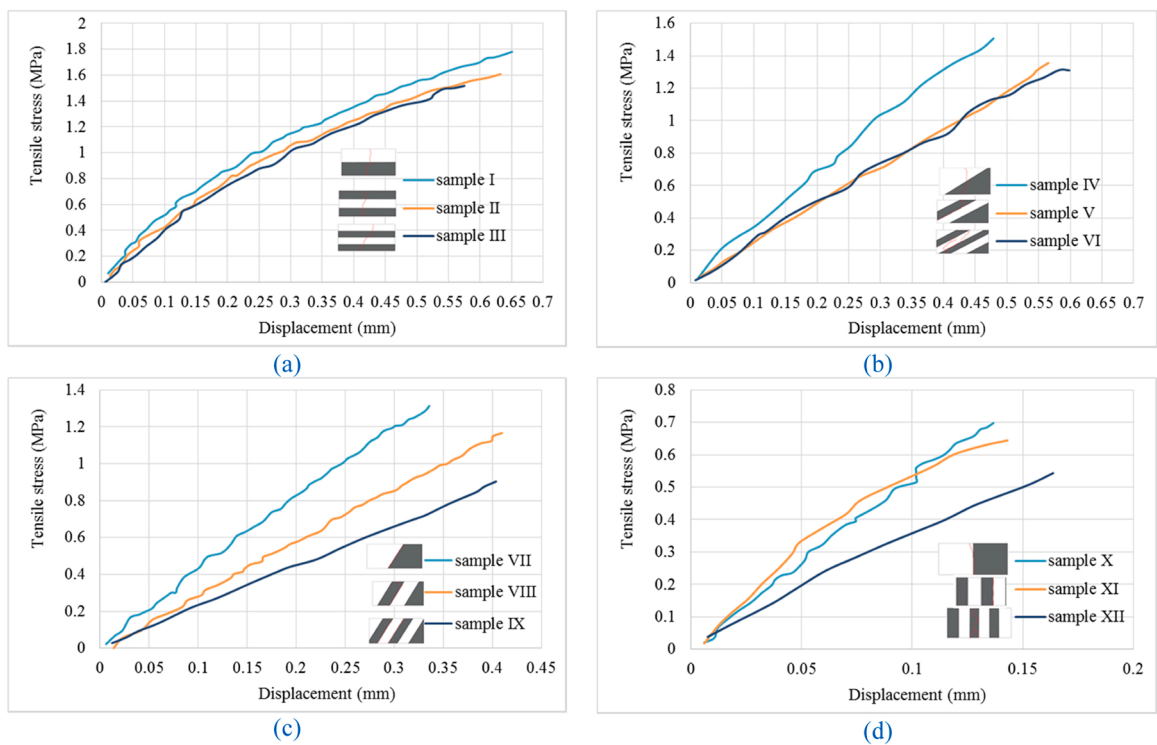


Fig. 8. Effects of bedding layer angle and bedding layer number on the stress- displacement curve.

rock mass deformation and failure [15,27,31]. For studying the deflections in the layered rock samples, the anisotropy behaviors of rock samples in the three-points load testing in necessary, which has not been deeply investigated in previous study. Therefore, in the present study, the anisotropy strength and failure modes of laminated concrete/gypsum using the three-point flexural test are investigated to evaluate the effects of concrete/gypsum bedding layers and their inclination angles on the tensile failure mechanism of specimens.

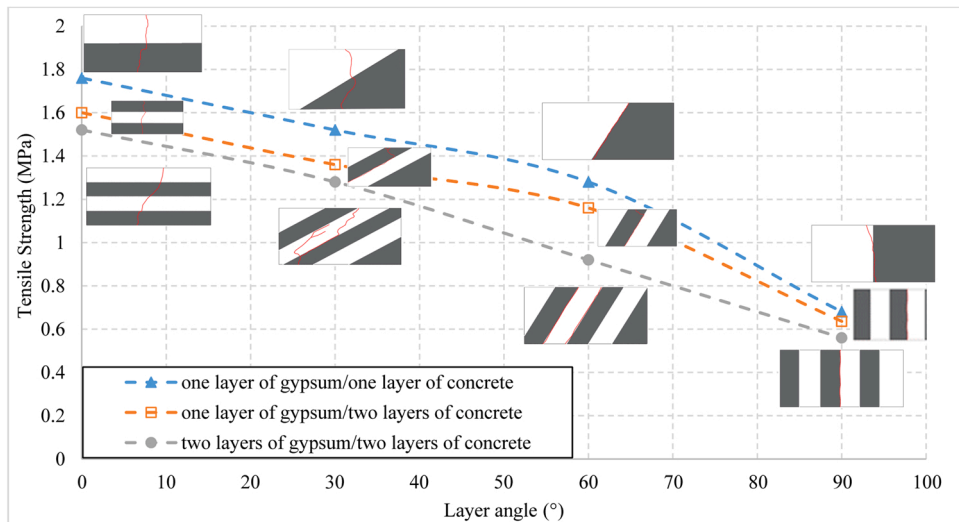






Fig. 9. The effect of bedding layer configuration and inclination angle on the tensile strength of concrete-gypsum specimens.

Table 6

Failure pattern of one layer of gypsum and one layer of concrete with different interface angle of (a) 0°, (b) 30°, (c) 60° and (d) 90°.

Angle (°)		Angle (°)	
0		30	
	(a)		(b)
60		90	
	(c)		(d)

2. Experimental program

2.1. Materials and mix design

The blocks including gypsum and concrete layers were prepared to be tested in three-point bending to simulate sedimentary type of rock. Generally, concrete is more robust than the gypsum; therefore, the combinations of concrete with gypsum represent the situation of rocks in the real world, which is rock masses with a high anisotropy ratio. Also, these material is easy assessable to repeat the test results. Gypsum was prepared by mixing gypsum and water with the ratio of 2:1. Gypsum consist of gypsum mineral ($\text{CaSO}_4 \cdot 2 \text{H}_2\text{O}$). The concrete mix included Portland cement, sand, gravel, water, superplasticizer and micro silica. Tables 1–3 summarize the mix design and specifications of different ingredients used in concrete specimens. Plastiment –BV 40 is the superplasticizer used in this study.

2.2. Mechanical properties of specimens

Indirect tensile strength test (Brazilian test) was conducted on the gypsum and concrete specimens with the diameter of 54 mm and thickness of 27 mm (Fig. 3) using Brazilian test machine (Fig. 4a).

The ultimate tensile strengths of concrete and gypsum were measured as 1.8 and 1.3 MPa, respectively. The crack growth of the

Table 7

Failure pattern of one layer of gypsum and two layers of concrete with different interface angle of (a) 0°, (b) 30°, (c) 60° and (d) 90°.






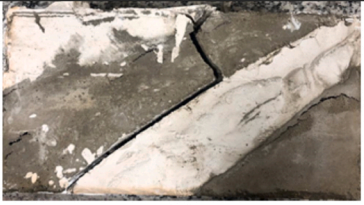


Angle (°)		Angle (°)	
0		30	
	(a)		(b)
60		90	
	(c)		(d)

Table 8

Failure pattern of two layers of gypsum and two layers of concrete with different interface angle of (a) 0°, (b) 30°, (c) 60° and (d) 90°.

Angle (°)		Angle (°)	
0		30	
	(a)		(b)
60		90	
	(c)		(d)

concrete and gypsum samples subjected to Brazilian tests are shown in Fig. 5a and b. Uniaxial compression test was conducted on the gypsum and concrete specimens with 300 * 160 * 75 (mm) dimension using uniaxial test machine (Fig. 4b) The ultimate compressive strengths of concrete and gypsum were measured as 20 MPa and 10 MPa, respectively. The crack growth of the concrete and gypsum samples subjected to uniaxial compressive strength tests are shown in Fig. 5c and d.

2.3. Sample preparation containing bedding layers

For this research project, the effects of concrete/gypsum bedding layers and their inclination angles on the tensile failure mechanism of specimens were evaluated via three-point bending test. Samples containing different layers of concrete and gypsum were prepared including one layer of gypsum and one layer of concrete, one layer of gypsum and two layers of concrete, and two layers of



Fig. 10. Different configuration of bedding layer above the underground gallery.

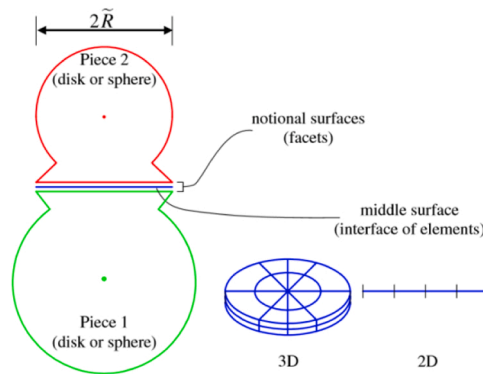


Fig. 11. Flat-joint model [56].

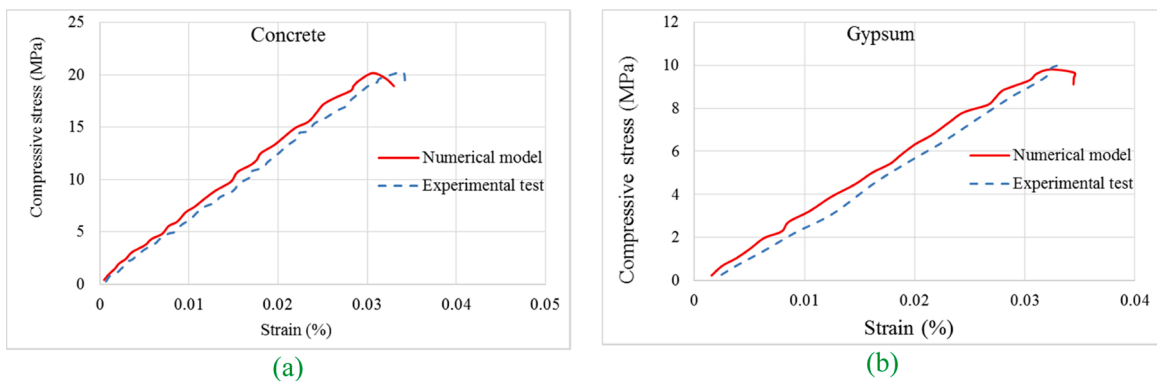


Fig. 12. stress-strain curve for a) intact concrete model and b) intact gypsum model.

gypsum and two layers of concrete as shown in Table 4. In each configuration, the angle of layers to the horizon varied at 0° , 30° , 60° and 90° . Entirely, 36 specimens including 12 types were prepared and tested (Sample I-XII in Table 4). Each test was repeated three times to ensure the accuracy of results and the average value was reported as the representing value.

The fresh gypsum and concrete were poured into the rectangle Plexiglas molds with the dimensions of $300 \times 150 \times 50$ mm (Fig. 6a) and then vibrated for 90 s to remove entrapped air. The molds were built from fiberglass to eliminate any changes in the dimensions during the sample preparation. Before pouring the mixed materials into the box, box was marked with guide line by a marker (Fig. 6a) based on the both of the angles between layers and layers thickness. The gypsum was poured into the mold according to the marked line. After initial solidification, concrete slurry was poured into the mold according to the marked line. As shown in Fig. 6b, for constructing the layers with specific angles and thickness, a rolling cylinder was moved below the mold to achieve the desired inclination angle and thickness. And whole system was built on the big container which filled with soil for controlling of the layers angle and thickness. The big container with soil was selected because it could change any directions and get any inclination. One cap was located at the top of the mold to hold the fresh mix in place (Fig. 6c). Fig. 3d, shows one sample containing four layers of

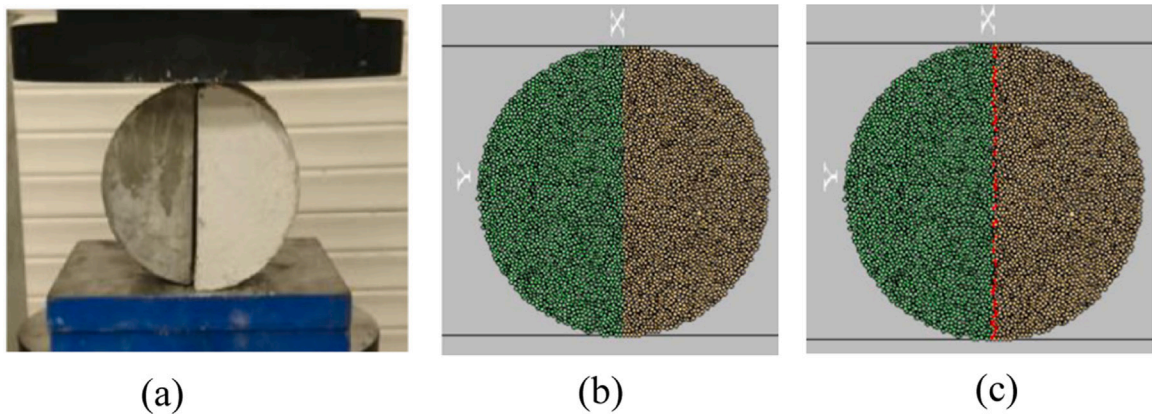


Fig. 13. Brazilian tests for determination of mechanical properties of gypsum-concrete interface [65].

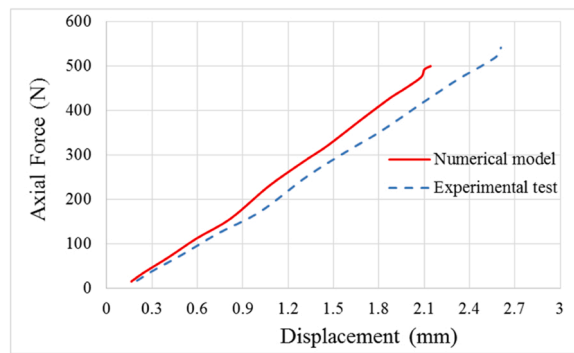


Fig. 14. Axial force versus Displacement curve for gypsum-concrete interface.

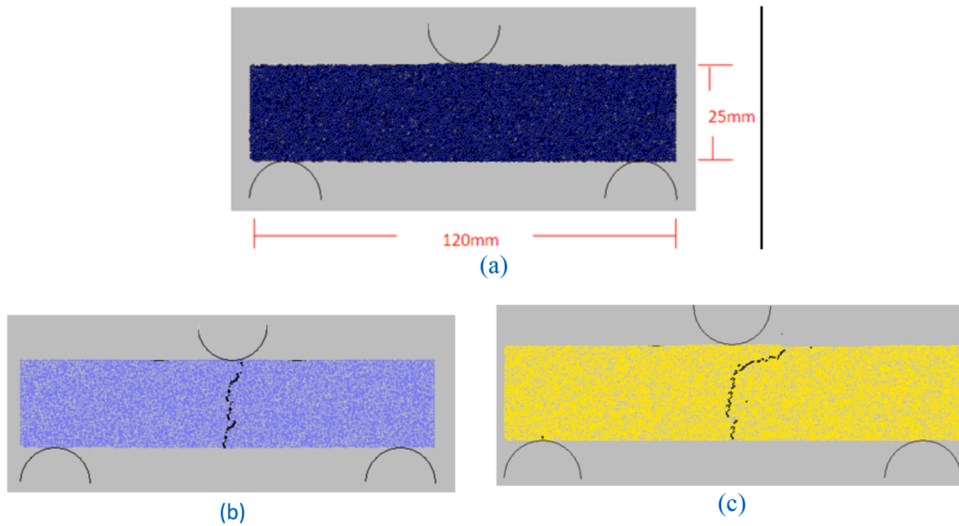
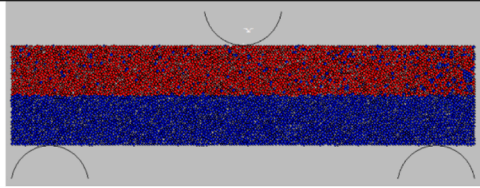
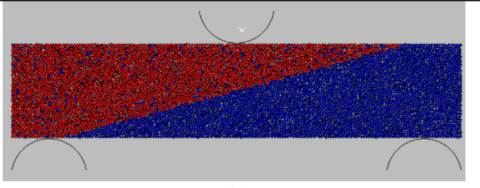
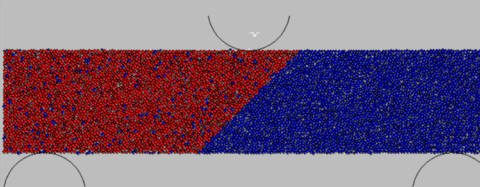
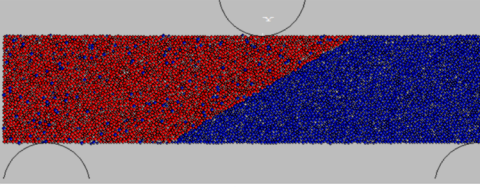
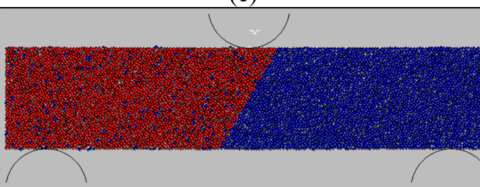
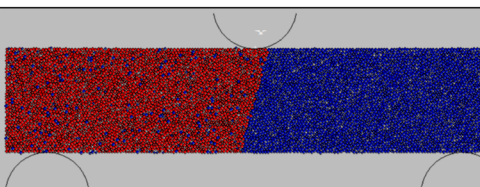
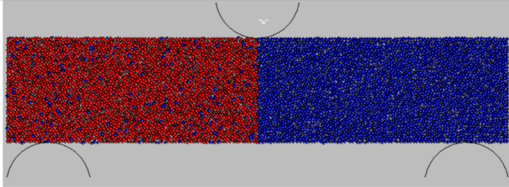


Fig. 15. (a) Model dimensions, (b) failure pattern of the gypsum model, and (c) failure pattern of the concrete model.

concrete and 4 layers of gypsum. Samples containing different combinations of concrete and gypsum layers (for horizontal configuration, it consisted of one layer of gypsum and one layer of concrete, one layer of gypsum and two layers of concrete, and two layers of gypsum and two layers of concrete) inclined at 0°, 30°, 60° and 90° were prepared as shown in Table 5.

Table 9
Gypsum/concrete model in PFC2D including one layer of gypsum and one layer of concrete with different interface angle.

Angle (°)		Angle (°)	
0		15	
30		45	
60		75	
90			

2.4. Three-point bending test (flexural strength test)

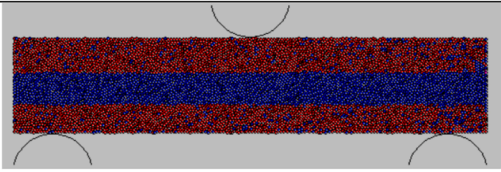
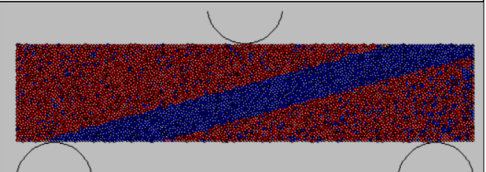
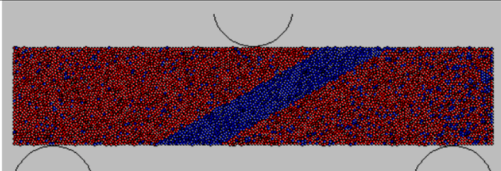
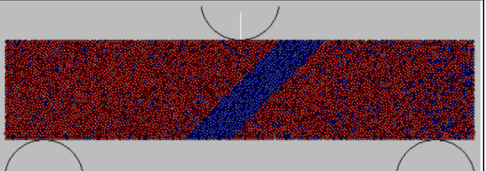
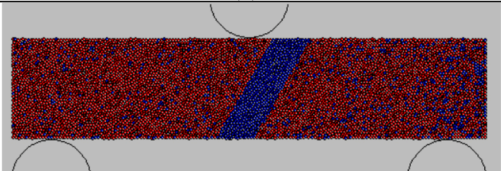
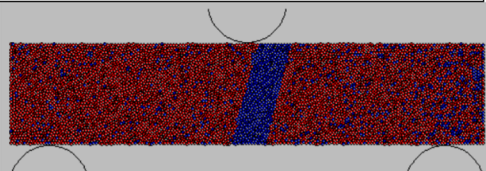
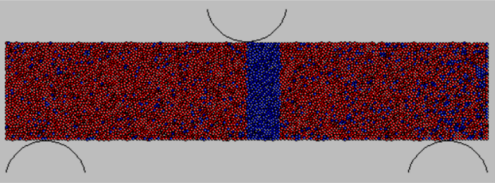
The specimens were tested in three-point bending after 28 days of curing to determine their flexural strength and their mechanical behaviors. The experimental arrangement for the flexural tests was according to the ASTM C78-16 [11]. For this arrangement, the cubic specimens were held by two sets of breaker near the end of its span. Hence, the prepared specimens were placed in the Y-axis utilizing two compressive wedges at a specific location. This arrangement stimulated the shear stress and permanent bending moment within the specific location. Individually, the normal tensile and compressive stresses emerged at the head and base of this central location. Besides, most of the substances have a specific amount of anisotropy in them. Bending strength in MPA (σ_{flex}) can be calculated using Eq. (1).

$$\sigma_{flex} = \frac{3WL}{4bd^2} \quad (1)$$

Where W is the maximum applied force, L is the distance between two loading point, b is the sample height and d is the sample width. In the tested specimens, L was 20 cm, b was 12 cm, and d was 10 cm. Two couples of steel wedges were installed in the lab equipment (see Fig. 7). The boundary condition for lower wedges was stationary to the machine, while the boundary condition of the top wedge was adjusted and controlled through a compressive platen. For applying the load on the specimens, the concrete-gypsum block samples were located in the uniaxial box (Fig. 7) and the rate of applied force was 0.005 mm/s.

Table 10

Gypsum/concrete model in PFC2D including one layer of gypsum and two layers of concrete with different interface angle.

Angle (°)		Angle (°)	
0		15	
	(a)		(b)
30		45	
	(c)		(d)
60		75	
	(e)		(f)
90			
	(g)		

3. Experimental results

3.1. Effects of bedding layer angle and bedding layer number on the stress- displacement curve

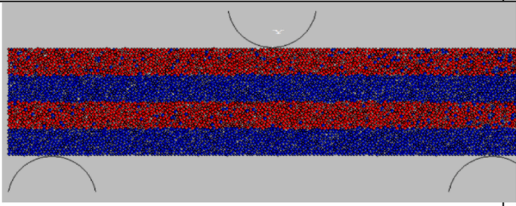
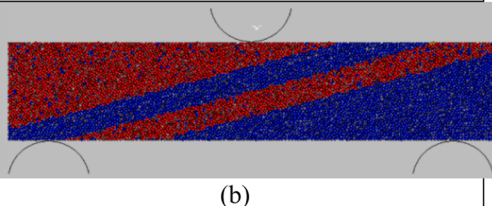
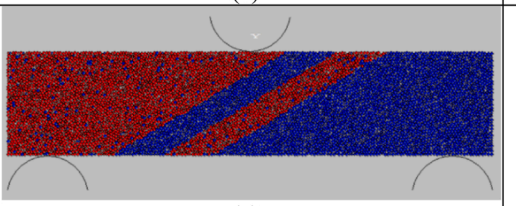
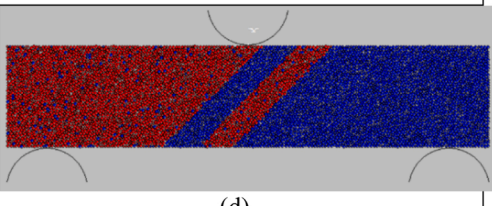
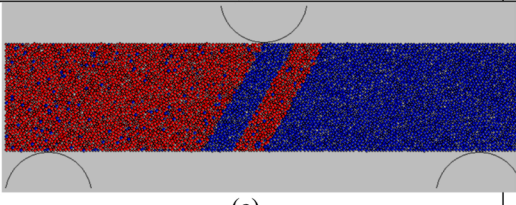
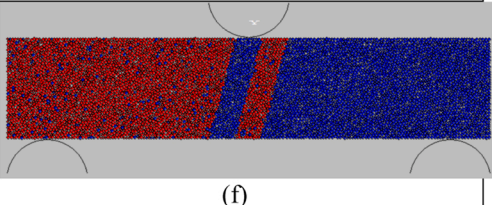
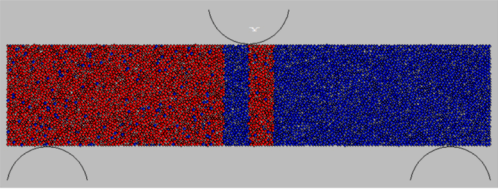
Fig. 8 shows the effects of bedding layer angle and bedding layer number on the stress- displacement curve. In constant layer angle, the maximum displacement associated to maximum stress was decreased by increasing the bedding number. When bedding layer angle was 0° , the average maximum displacement was 0.6 mm while it was 0.12 for layer angle of 90° . Therefore it can be concluded that the average maximum displacement was decreased by increasing the bedding angle. The stress-displacement curve was non-linear for layer angle of 0° while it was linear for layer angle of 90° . Because the intact material was mobilized in failure processes for layer angle of 0° while the layer interfaces was mobilized for layer angle of 90° .

3.2. Effects of bedding layers on the tensile strength

Fig. 9. Shows the effect of bedding layers on the tensile strength. As can be seen, the tensile strength decreased by increasing the bedding layer numbers because of increasing the number of weak layers in specimens. Keeping the layer angle fixed, the highest tensile strength belonged to the case with one layer of concrete and one layer of gypsum, which is intuitively expected due to the involvement of the lowest number of interfaces. In addition, the tensile strength decreased by increasing the bedding layer angle, which is due to decreasing the angle between loading direction and bedding plane. The specimen including one layer of concrete and one layer of gypsum inclined at 0° had the highest tensile strength (1.8 MPa). However, the lowest tensile strength (0.56 MPa) belonged to the specimen including two layers of gypsum and two layers of concrete inclined at 90° , when the loading direction was parallel to the weak plane. Considering the effects of bedding layer and their inclination angle, it can be concluded that the effect of inclination of bedding layer is more significant on the tensile strength of specimens comparing to the number of bedding layers. As the inclination angle reaches 90° , the tensile strength of specimens becomes less sensitive to the number of layers because, in this configuration, only

Table 11

Gypsum/concrete model in PFC2D including two layers of gypsum and two layers of concrete with different interface angle.

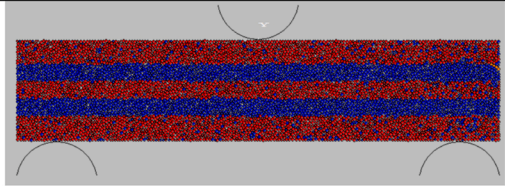
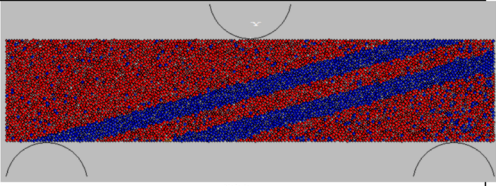
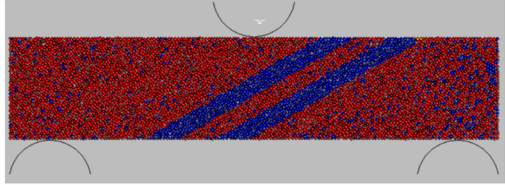
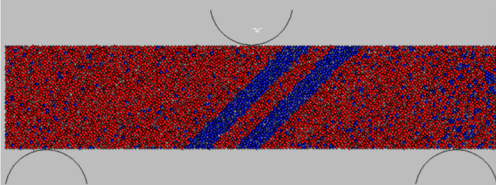
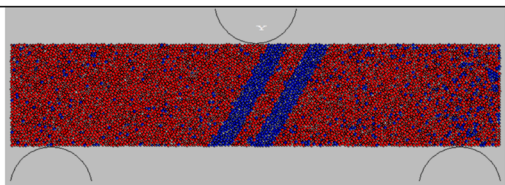
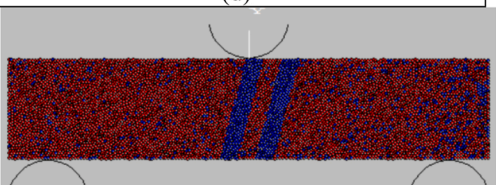
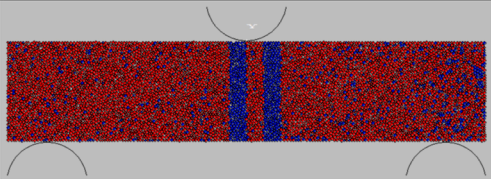
Angle ($^{\circ}$)		Angle ($^{\circ}$)	
0		15	
	(a)		(b)
30		45	
	(c)		(d)
60		75	
	(e)		(f)
90			
	(g)		

one tensile failure surface developed through the model by increasing the layers number. However, for the other inclinations, the failure surface number changed by increasing the layers number.

3.3. Crack growth in concrete-gypsum blocks

Tables 6–8 show the crack growth of concrete-gypsum blocks. In the samples of this research, two kinds of failure modes were detected. When the interface angle was 0° and 30° (Tables 6–8 a and b), one tensile crack was initiated in the gypsum and developed in the vertical direction until coalescence with gypsum-concrete interface. In other words, the failure mode is autonomous of layers (AL), whereby fractures occur in the central zone of the samples. This tensile crack propagated parallel to loading axis again and went through the concrete layer until coalescence with gypsum boundary. When the interface angle was 60° (Tables 6–8c), one tensile crack initiated in the concrete-gypsum interface and propagated diagonally until joining the cracks in the top edge of the sample. When the interface angle was 90° (Tables 6–8d), one tensile crack initiated in the concrete-gypsum interface and grew in the vertical direction until joined the cracks in the top edge of sample. In other words, the failure mode is dependent of layers, whereby fractures occur in the concrete-gypsum interface zone of the samples. When the interface angle was 90° , the loading direction was similar to the joint plane. Therefore, the crack propagated along this weaker zone. The fracturing pattern outcomes in the concrete-gypsum blocks seem to be compatible with the results of Khanlari et al. [40]. They investigated the crack growth of the two types of sandstone under an indirect tensile test. The shift in the crack pattern based on the three-point bending test values is also observed in other studies. Khanlari et al. [40] showed the alteration of the fracture pattern in BTS samples (Brazilian Tensile Strength) of sandstone at layers angle = 45° .

Table 12
Gypsum/concrete model in PFC2D including two layers of gypsum and three layers of concrete with different interface angle.

Angle (°)		Angle (°)	
0		15	
	(a)		(b)
30		45	
	(c)		(d)
60		75	
	(e)		(f)
90			
	(g)		

3.4. Behavior of bedding layer above the underground space

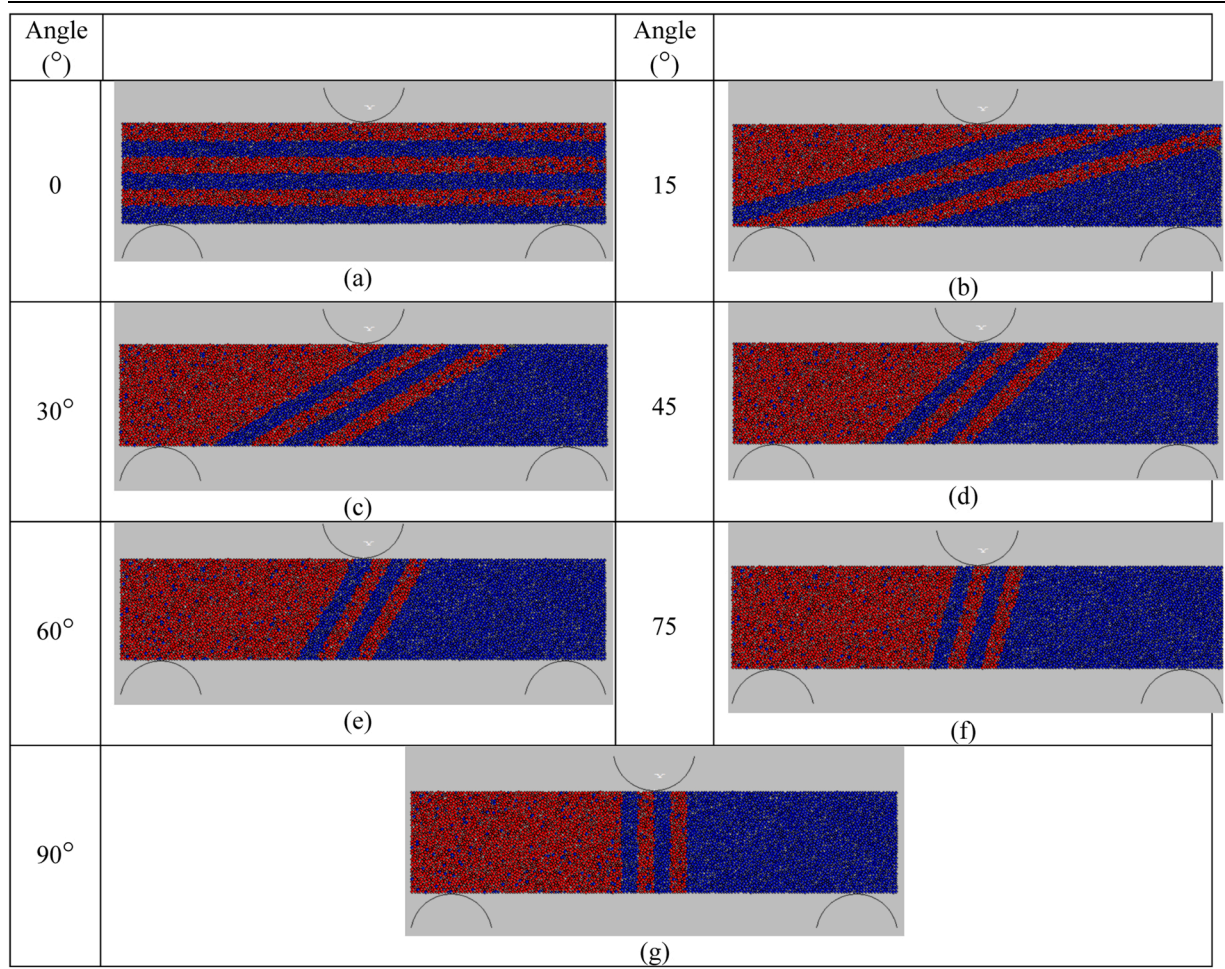
Fig. 10 shows different configuration of bedding layer above the underground gallery. From above findings, it can be concluded that model I and model XII have highest tensile strength and lowest tensile strength, respectively. Model I can deformed largely before final failure while model XIII has a small deformation before final failure. Therefore model XIII is a critical condition for bedding layer.

4. Numerical simulation

4.1. Particle Flow Code

A polygonal grain arrangement of balls was taken into account by [57] to develop the flat joint (FJ) model. According to Fig. 11, FJ contacts are modeled as inflexible balls that are rigidly connected to flat notional surfaces. The notional surface of each piece is its face, and the face of the contacting piece is its notional surface. Therefore, faces on grains were represented as two-dimensional or three-dimensional balls with skirts. In two-dimensional, these faces are lines, while in three-dimensional, they are disks. The phrase (FJM) flat-jointed material refers to what is known as a ball assembly held together by FJ contacts. Faceted grains can be discretized into elements, with some pieces being bonded and some unbonded. The FJs are then established at grain-to-grain contact with force and torque set to zero at each element and are varied according to the force-displacement law of bonding and relative motions between faces. Shear forces were adjusted incrementally, while normal forces were adjusted directly. It will behave linearly as long as the bonded element's strength remains under its limit. An element's normal and shear stress maximum is measured $(\sigma_{max}^{(e)}, \tau_{max}^{(e)})$ based on the following:

Table 13
Gypsum/concrete model in PFC2D including three layers of gypsum and three layers of concrete with different interface angle.



$$\sigma_{max}^{(e)} = \frac{-\bar{F}_{(e)}^n}{A^{(e)}} \tag{2}$$

$$\tau_{max}^{(e)} = \frac{\bar{F}_{(e)}^s}{A^{(e)}} \tag{3}$$

Where $\bar{F}_{(e)}^n$ and $\bar{F}_{(e)}^s$ are normal and shear loads applied on the element, and $A^{(e)}$ is the element area, respectively. A unique arrangement of faced grains supplied elements with excellent rotational resistance and comparatively no torque contribution. Coulomb criterion with tension cut-off was utilized to calculate the strength of bonded elements. When normal stress overreaches to the element tensile strength ($\sigma_{max}^{(e)} > \sigma_b$), the element breaks in tension, causing tensile cracks to form and the element phase change to unbonded. Cohesion c and friction angle \varnothing_b determine an element's shear strength. When shear stress overreaches to the element's shear strength [$\tau_{max}^{(e)} > \tau_c = c_b - \bar{\sigma} \tan \varnothing_b$], the bond breaks in shear, and the bond phase altered to unbonded. Linear elastic with frictional slip is the mechanical behavior of unbonded elements. The following is the force-displacement law:

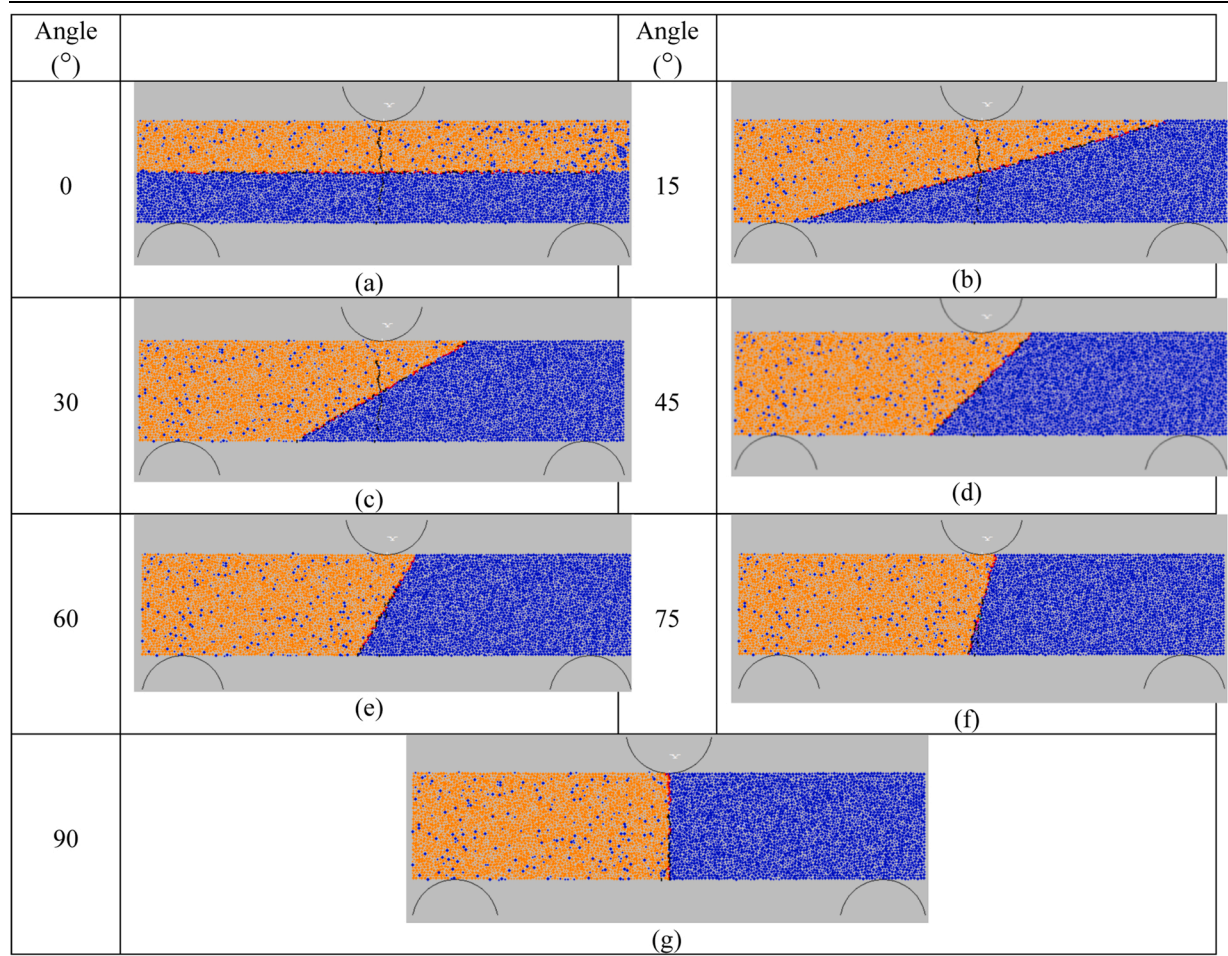
$$\bar{\sigma} = \begin{cases} 0 & \bar{g} \geq 0 \\ -k_n \bar{g} & \bar{g} < 0 \end{cases} \tag{4}$$

$$\bar{\tau} = \begin{cases} -\bar{\sigma} \tan \varnothing_r & -\bar{\sigma} < 0 \\ 0 & -\bar{\sigma} = 0 \end{cases} \tag{5}$$

Where \bar{g} the element is gap, and \varnothing_r is the residual friction angle of unbonded element. The FJ contact suffers some damage as a result of the breakage of each bonded element. As soon as a FJ contact is displaced beyond its diameter, the faces are removed, and the linear

Table 14

Failure pattern of gypsum/concrete model in PFC2D including one layer of gypsum and one layer of concrete with different interface angle.



contact model is applied if these particles come back into contact again [56,58, 59].

4.2. Preparation and calibration of the DEM Model

For calibrating the micro-mechanical feature of intact concrete and gypsum the trial-error approach by [68,71] was used. Fig. 12a and b shows the stress-strain curve for both of the intact concrete model and intact gypsum model. The results shows the well matching between the numerical simulation and experimental test.

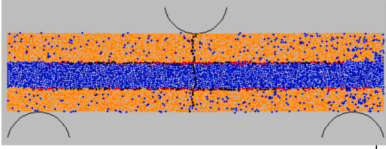
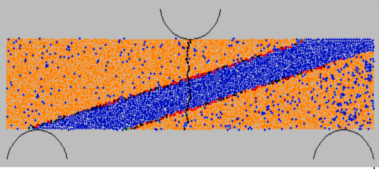
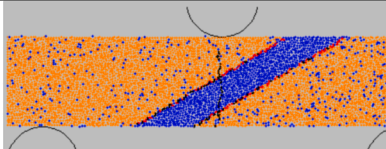
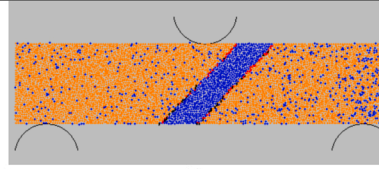
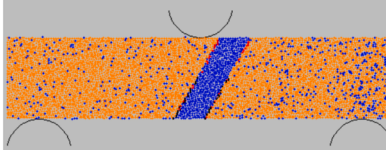
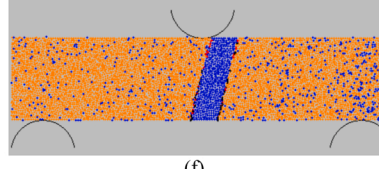
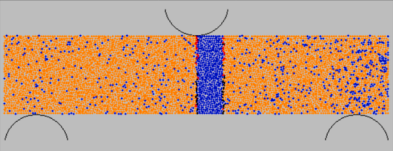
4.3. Numerical simulations on the gypsum–concrete interface

After calibration of PFC2D, Brazilian tests for determination of mechanical properties of gypsum–concrete interface were experimentally tested and numerically simulated by creating two semi-circular model (by using the calibrated micro-parameters) as shown in Fig. 13. The PFC2D specimen had a diameter of 100 mm. The micro-parameters for gypsum and concrete were applied into the model, considering 50 % of the model as gypsum and the other 50 % as concrete. Micro-properties for layer interfaces were also chosen by try and error method to obtain the best results close to the experimental outcome. Therefore, the normal bond (n_bond), shear bond (s_bond) and friction coefficient were considered as 1000 MPa, 1000 MPa, and 0.25, respectively. The red line in Fig. 13c represents the tensile crack created in gypsum–concrete specimen under loading. By comparing Fig. 13a and c, it can be concluded that the tensile fracture occurs in interface of gypsum/concrete sample. The failure load was measured as 1000 N.

Fig. 14 shows the axial force versus axial displacement for gypsum–concrete interface in experimental test and numerical simulation. The results shows the well matching between the numerical simulation and experimental test. It could be concluded that the numerical model was calibrated correctly.

Table 15

Failure pattern of gypsum/concrete model in PFC2D including one layer of gypsum and two layers of concrete with different interface angle.

Angle (°)		Angle (°)	
0		15	
	(a)		(b)
30		45	
	(c)		(d)
60		75	
	(e)		(f)
90			
	(g)		

4.4. Numerical simulation of intact gypsum and intact concrete specimens under three point bending

The tensile strength of gypsum and concrete specimens were calibrated for numerical simulation in three point bending test. The dimensions of the rectangular samples were 120 mm (width) and 25 mm (height) as shown in Fig. 15a. The tensile crack shown by a black line represents the failure pattern of both intact rectangular gypsum and concrete specimens in Fig. 15b and c, respectively. In gypsum models, the tensile crack was initiated from lower part of the model and propagated parallel to loading axis till coalescence with model boundary (Fig. 15b). In concrete models, the tensile crack was initiated from lower part of the model and propagated parallel to loading axis. This crack was rotated toward the right side of the upper loading wall and coalescence to model boundary (Fig. 15c). The ultimate tensile strength of concrete and gypsum under three-point bending test in numerical simulation were determined as 1.7 and 1.2 MPa, respectively.

4.5. Model development by Particle Flow Code

After model calibration, a box model with dimension of 120 mm × 25 mm in PFC2D including layers of concrete and gypsum were simulated to be tested under three-point bending tests as shown in Tables 9–13. A total of 7179 balls with 0.54 mm diameter were utilized to make the sample. Models containing different combinations of concrete and gypsum layers were prepared i.e. one layer of gypsum and one layer of concrete (Table 9), one layer of gypsum and two layers of concrete (Table 10), two layers of gypsum and two layers of concrete (Table 11), two layers of gypsum and three layers of concrete (Table 12) and three layers of gypsum and three layers of concrete (Table 13). In each configuration, bedding layer angles changed from 0° to 90° with increment of 15°. Totally 35 models were simulated and subjected to three point bending (Tables 9–13) to examine their mechanical behaviors.

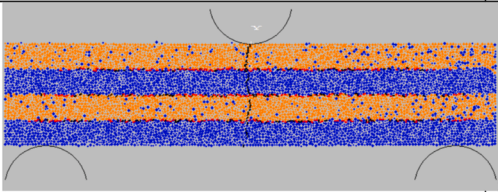
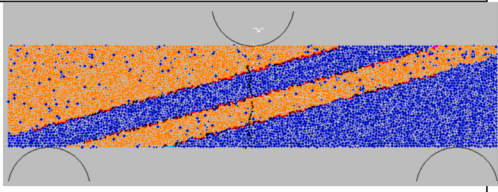
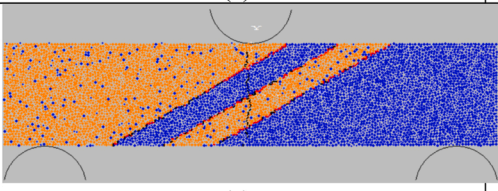
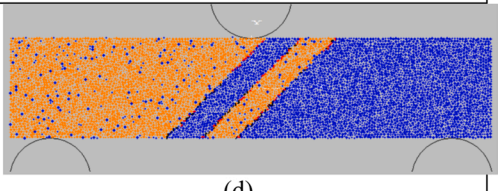
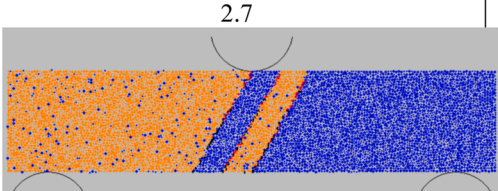
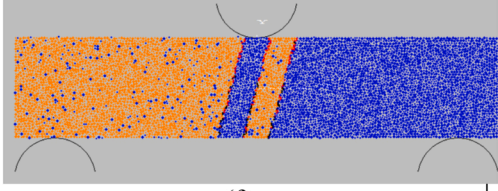
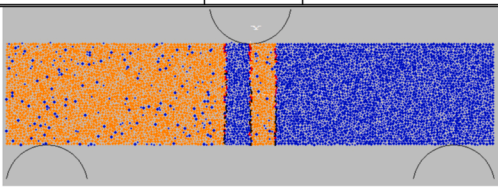
5. Results

5.1. Failure pattern of concrete- gypsum blocks in numerical simulation

Tables 14–18 show the failure pattern of the concrete- gypsum blocks in numerical simulation. When the interface angles were 0°, 15° and 30°, one tensile crack initiated in concrete and propagated in the vertical direction until reaching the gypsum-concrete interface. In other words, the failure mode is autonomous of layers (AL), whereby fractures occur in the central zone of the

Table 16

Failure pattern of gypsum/concrete model in PFC2D including two layers of gypsum and two layers of concrete with different interface angle.

Angle (°)		Angle (°)	
0		15	
	(a)		(b)
30		45	
	(c)		(d)
60		75	
	(e)		(f)
90			
	(g)		

samples. This tensile crack propagated parallel to the loading axis and went through the gypsum layer until coalescence with gypsum boundary. We want to emphasize that unusual tensile cracks developed in the interface of concrete-gypsum layers. This trend was observed in the other combination of concrete and gypsum layers with interface angles of 0°, 15° and 30° (Tables 14–18). When the interface orientations were 45°, 60°, 75° and 90° (Table 14), one tensile fracture initiated in the boundary of concrete-gypsum layers and propagated in the concrete-gypsum interface until coalescence with the upper boundary of sample. In other words, the failure mode is dependent of layers, whereby fractures occur in the concrete-gypsum interface zone of the samples. This trend was observed in the other combination of concrete and gypsum layers with interface angles of 45°, 60°, 75° and 90° (Tables 14–18).

5.2. The relationship of the orientation layers and the tensile strength of concrete/gypsum specimens in numerical simulation

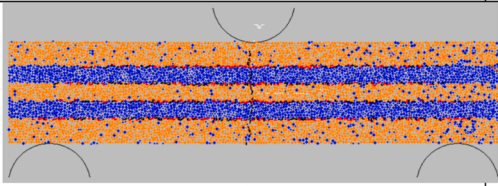
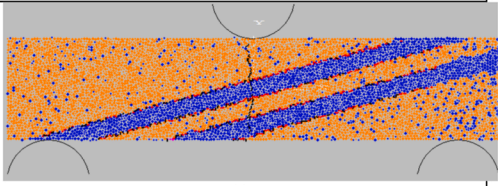
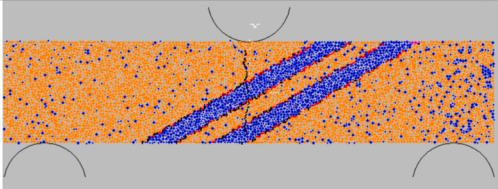
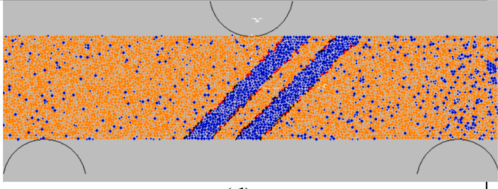
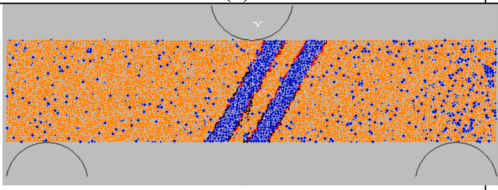
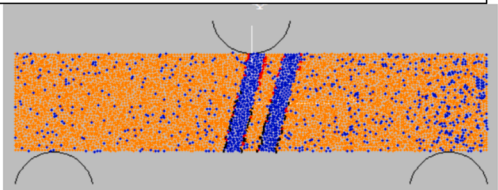
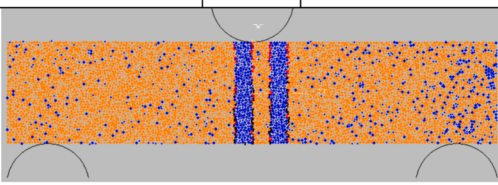
Fig. 16 shows the effect of concrete/gypsum bedding layers on the tensile strength of specimens in numerical simulation. As can be seen, the tensile strength of specimens increased by increasing the bedding layer thickness (decreasing the number of layers). In addition, tensile strength decreased by increasing the bedding layer angle. Therefore, the specimen with one layer of concrete and one layer of gypsum and 0° inclination angle had the highest tensile strength.

6. Conclusion

The effects of different concrete/gypsum layer numbers and their inclination angles on the tensile strength and failure pattern of the gypsum-concrete blocks were studied in the three point bending test using experimental tests and numerical simulation. The results from this study can be summarized as:

Table 17

Failure pattern of gypsum/concrete model in PFC2D including two layers of gypsum and three layers of concrete with different interface angle.

Angle (°)		Angle (°)	
0		15	
30		45	
60		75	
90			

- Under three-point bending test conditions and numerical simulation, the concrete/gypsum layer's crack patterns depend significantly on the layers' orientation.
- The three-point bending test results show that samples with one layer of concrete and gypsum with layer angle less than 30° (1.76 MPa) have higher tensile strength than samples with layer angle more than 30° (1.52 MPa). This follows the anticipation that when the layer orientation is horizontal or sub horizontal layer angle less than 30°, the cracks mostly cross the layers, but with increasing layer orientation layer angle to more than 30°, the cracks appear alongside the layer. In other words, the cracks appeared in the weaker mechanical properties zone.
- Two significant ways of fracture patterns were detected in the concrete-gypsum blocks of this study. For layer angle less than 30°, the failure mode is autonomous of layers (AL) (fractures occur parallel to the loading direction). For layer angle > 30°, failure mode depends on layers (cracks appeared in the interface of the layer).
- In constant layer angle, the maximum displacement associated to maximum stress was decreased by increasing the bedding number. The stress-displacement curve was non-linear for layer angle of 0° while it was linear for layer angle of 90°.
- By reducing the number of layers in the sample, the tensile strength increases.
- Tensile strength decreases by increasing the bedding layer angle.
- As the inclination angle reaches to 90°, the tensile strength of specimens become close to each other because in this configuration, only one tensile failure surface developed through the model by increasing the layers number. However, in other inclination, the failure surface number changed by increasing the layers number.
- The failure patterns achieved in the numerical simulations are in good agreement with the experimental data (Table 14a, c, e and g, Table 15a, c, e and g and Table 16a, c, e and g) and experimental tests (Table 5).
- Tensile strengths are approximately identical in both the numerical simulations and experimental tests (one layer gypsum/one layer concrete-one layer gypsum/two layer concrete- two layer gypsum/two layer concrete).

Table 18

Failure pattern of gypsum/concrete model in PFC2D including three layers of gypsum and three layers of concrete with different interface angle.

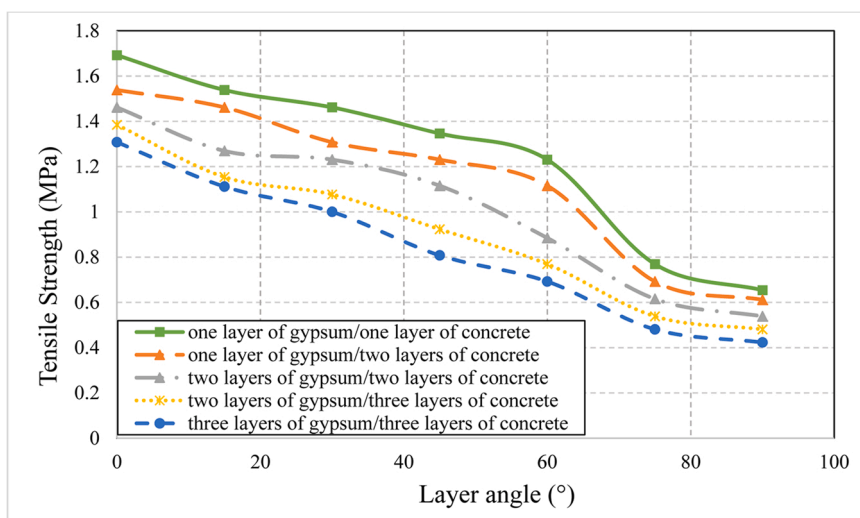
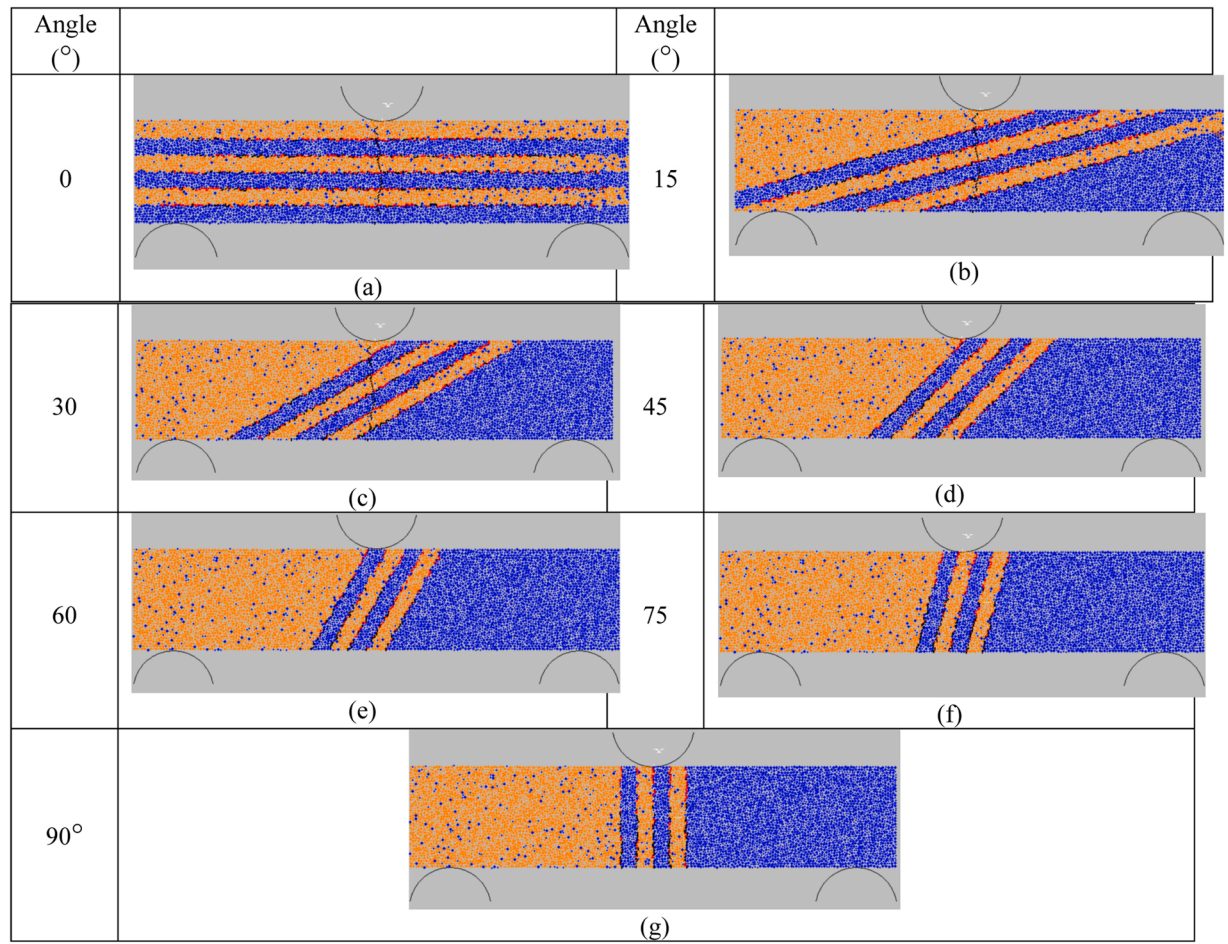


Fig. 16. The effect of bedding layer on the tensile strength of concrete/gypsum specimens in PFC2D.

Declaration of Competing Interest

The authors declare that they have no known competing financial interests or personal relationships that could have appeared to influence the work reported in this paper.

Data availability

The data that has been used is confidential.

References

- [1] ASTM C78–16. Standard Test Method for Flexural Strength of Concrete (Using Simple beam with Third-Point Loading), ASTM International, West Conshohocken, 2016.
- [2] R. Ajalloeian, G.R. Lashkaripour, Strength anisotropies in mudrocks, *Bull. Eng. Geol. Environ.* 59 (2000) 195–199.
- [3] A.A. Al-Harhi, Effect of planar structures on the anisotropy of Ranyah sandstone, Saudi Arabia, *Eng. Geol.* 50 (1998) 49–57.
- [4] B. Amadei, Importance of anisotropy when estimating and measuring in situ stresses in rock, *Int. J. Rock. Mech. Min. Sci. Geomech. Abstr.* (1996) 293–325.
- [5] N.A. Al-Shayea, K. Khan, S.N. Abduljawad, Effects of confining pressure and temperature on mixed-mode (I-II) fracture toughness of a limestone rock, *Int. J. Rock. Mech. Min. Sci.* 37 (2000) 629–643, [https://doi.org/10.1016/S1365-1609\(00\)00003-4](https://doi.org/10.1016/S1365-1609(00)00003-4).
- [6] M.R.M. Aliha, M.R. Ayatollahi, D.J. Smith, M.J. Pavier, Geometry and size effects on fracture trajectory in a limestone rock under mixed mode loading, *Eng. Fract. Mech.* 77 (2010) 2200–2212, <https://doi.org/10.1016/j.engfracmech.2010.03.009>.
- [7] A. Basu, M. Kamran, Point load test on schistose rocks and its applicability in predicting uniaxial compressive strength, *Int. J. Rock. Mech. Min. Sci.* 47 (2010) 823–828.
- [8] T. Bai, D.D. Pollard, Closely spaced fractures in layered rocks: initiation mechanism and propagation kinematics, *J. Struct. Geol.* 22 (10) (2000) 1409–1425.
- [9] M.H.N. Behrestaghi, K.S. Rao, T. Ramamurthy, Engineering geological and geotechnical responses of schistose rocks from dam project areas in India, *Eng. Geol.* 44 (1996) 183–201.
- [10] E. Broch, Estimation of strength anisotropy using the point load test, *Int. J. Rock. Mech. Min. Sci.* 20 (1983) 181–187.
- [11] E. Broch, J.A. Franklin, The point load strength test, *Int. J. Rock. Mech. Min. Sci.* 9 (1972) 669–697.
- [12] M.E. Chenevert, C. Gatlin, Mechanical anisotropies of laminated sedimentary rocks, *Soc. Pet. Eng. J.* 5 (1965) 67–77.
- [13] G.J. Chen, T. Maes, F. Vandervoort, X. Sillen, V.P. Marcke, M. Honty, M. Dierick, P. Vanderniepen, Thermal impact on damaged boom clay and opalinus CLAY: permeability and isostatic tests with μ CT scanning, *Rock. Mech. Rock. Eng.* 47 (2014) 87–99.
- [14] C.S. Chen, E. Pan, B. Amadei, Determination of deformability and tensile strength of anisotropic rock using Brazilian tests, *Int. J. Rock. Mech. Min. Sci.* 35 (1) (1998) 43–61.
- [15] J. Coggan, F. Gao, D. Stead, D. Elmo, Numerical modelling of the effects of weak immediate roof lithology on coal mine roadway stability, *Int. J. Coal Geol.* 90 (2012) 100–109.
- [16] J.W. Cho, H. Kim, S. Jeon, K.B. Min, Deformation and strength anisotropy of Asan gneiss, Boryeong shale, and Yeoncheon schist, *Int. J. Rock. Mech. Min. Sci.* 50 (2012) 158–169.
- [17] P.M. Douglass, B. Voight, Anisotropy of granites: a reflection of microscopic fabric, *Geotechnique* 19 (3) (1969) 376–379.
- [18] F. Dai, K. Xia, M. Nasser, Micromechanical model for the rate dependence of the fracture toughness anisotropy of Barre granite, *Int. J. Rock. Mech. Min. Sci.* 63 (2013) 113–121, <https://doi.org/10.1016/j.ijrmm.2013.08.011>.
- [19] B. Debecker, A. Vervoort, Experimental observation of fracture patterns in layered Slate, *Int. J. Fract.* 159 (2009) 51–62.
- [20] F. Dai, K. Xia, Tensile strength anisotropy of Barre granite, *Pure Appl. Geophys* 167 (2010) 1419–1432.
- [21] F. Dai, K. Xia, M.H.B. Nasser, Laboratory measurements of the rate dependence of the fracture toughness anisotropy of Barre granite, *Int. J. Rock. Mech. Min. Sci.* 60 (2013) 57–65.
- [22] F. Dai, K. Xia, J.P. Zuo, R. Zhang, N.W. Xu, Static and dynamic flexural strength of anisotropic Barre granite, *Rock. Mech. Rock. Eng.* 46 (2013) 1589–1602.
- [23] F.A. Donath, *Strength variation and deformational behaviour of anisotropic rocks. State of Stress in the Earth's Crust*, Elsevier, New York, 1964.
- [24] Deklotz E.J., Brown J.W., Stemler O.A., 1966, Anisotropy of a schistose gneiss, in: *Proceedings of the First Congress of International Society of Rock Mechanics*, Lisbon, 465–470.
- [25] D.Q. Dan, H. Konietzky, Numerical simulations and interpretations of Brazilian tensile tests on transversely isotropic rocks, *Int. J. Rock. Mech. Min. Sci.* 71 (2014) 53–63.
- [26] K. Duan, C.Y. Kwok, Discrete element modeling of anisotropic rock under Brazilian test conditions, *Int. J. Rock. Mech. Min. Sci.* 78 (2015) 46–56.
- [27] Elmo, D.; Clayton, C.; Rogers, S.; Beddoes, R.; Greer, S., Numerical simulations of potential rock bridge failure within a naturally fractured rock mass, in: *Proceedings of the International Symposium on Slope Stability in Open Pit Mining and Civil Engineering*, Vancouver, BC, Canada, 18–21 September 2011, Eberhardt, E.S.D., Ed.
- [28] Esterhuizen G.S., Dolinar D.R., Ellenberger J.L., Prosser L.J., Iannacchione A.T., Roof stability issues in underground limestone mines in the United States, in: *Proceedings of the Twenty Sixth International Conference on Ground Control in Mining*, Morgantown WV, West Virginia University, 2007, 320–27.
- [29] Funatsu, T., Takashi, T., Kuruppu, M., 2012. Effect of anisotropy on fracture toughness of sandstone by SCB specimen, in: *Proceedings of the ARMS7–Seventh Asian Rock Mechanics Symposium*, Seoul, South Korea, 413–418.
- [30] D. Guha Roy, T.N. Singh, Effect of heat treatment and layer orientation on the tensile strength of a crystalline rock under Brazilian test condition, *Rock Mech. Rock Eng.* 49 (5) (2016) 1663–1677, <https://doi.org/10.1007/s00603-015-0891-y>.
- [31] F. Gao, D. Stead, J. Coggan, Evaluation of coal longwall caving characteristics using an innovative UDEC Trigon approach, *Comput. Geotech.* 55 (2014) 448–460.
- [32] Guha Roy, D., Singh, T.N., Kodikara, J., 2016. Correlating fracture properties of saturated sedimentary rocks with compressive strength, in: *Proceedings of the Ninth Asian Rock Mechanics Symposium*, Bali, Indonesia, ARMS9-PO6-P108.
- [33] P.K. Gautam, A.K. Verma, S. Maheshwar, T.N. Singh, Thermomechanical analysis of different types of sandstone at elevated temperature, *Rock. Mech. Rock. Eng.* 49 (5) (2016) 1985–1993, <https://doi.org/10.1007/s00603-015-0797-8>.
- [34] Ghamgosar, M., Williams, D.J., Erarslan, N., 2015. Effect of anisotropy on fracture toughness and fracturing of rocks, in: *Proceedings of the Fiftieth US Rock Mechanics/Geomechanics Symposium*. ARMA, Houston, 15–634.
- [35] D.W. Hobbs, The tensile strength of rocks, *Int. J. Rock. Mech. Min. Sci.* 1 (1963) 385–396.
- [36] F.G. Horino, M.L. Ellickson, A method of estimating the strength of rock containing planes of weakness. US Bureau Mines Itasca Consulting Group, Inc., 2004. Particle Flow Code in 2-Dimensions: Problem Solving with PFC2D, Version 3.1, Itasca Consulting Group, Inc., Minneapolis, 1970.
- [37] C.L. John, L.S. Jenny, S.S. David, Natural fractures in the Spraberry formation, Midland basin, Texas: the effect of mechanical stratigraphy on fracture variability and reservoir behavior, *AAPG Bull.* 86 (3) (2002) 505–524.
- [38] K.Y. Kim, L. Zhuang, H. Yang, H. Kim, K.B. Min, Strength anisotropy of Berea sandstone: results of X-ray computed tomography, compression tests, and discrete modeling, *Rock. Mech. Rock. Eng.* 49 (2016) 1201–1210.
- [39] A. Khosravi, R. Simon, P. Rivard, The shape effect on the morphology of the fracture surface induced by the Brazilian test, *Int. J. Rock. Mech. Min. Sci.* 93 (2017) 201–209.

- [40] G. Khanlari, B. Rafiei, Y. Abdilor, An experimental investigation of the Brazilian tensile strength and failure patterns of laminated sandstones, *Rock. Mech. Rock. Eng.* 48 (2015) 843–852.
- [41] G.R. Khanlari, M. Heidari, A.A. Sepahi, D. Fereidooni, Determination of geotechnical properties of anisotropic rocks using some index tests, *Geotech. Test. J.* 37 (2) (2013) 1–13, <https://doi.org/10.1520/GTJ20130078>.
- [42] G.R. Khanlari, M. Heidari, A.A. Sepahi, D. Fereidooni, Quantification of strength anisotropy of metamorphic rocks of the Hamedan prov- ince, Iran, as determined from cylindrical punch, point load and Brazilian tests, *Eng. Geol.* 169 (2014) 80–90.
- [43] M.D. Kuruppu, Y. Obara, M.R. Ayatollahi, K.P. Chong, T. Funatsu, ISRM-suggested method for determining the mode I static fracture toughness using semi-circular bend specimen, *Rock. Mech. Rock. Eng.* 47 (2014) 267–274, <https://doi.org/10.1007/s00603-013-0422-7>.
- [44] M.F. Lei, L.M. Peng, C.H. Shi, S.Y. Wang, Experimental study on the damage mechanism of tunnel structure suffering from sulfate attack, *Tunn. Undergr. Space Technol.* 36 (2013) 5–13.
- [45] V. Labiouse, T. Vietor, Laboratory and in situ simulation tests of the excavation damaged zone around galleries in Opalinus clay, *Rock. Mech. Rock. Eng.* 47 (2014) 57–70.
- [46] A. Lisjak, B. Garitte, G. Grasselli, H.R. Müller, T. Vietor, The excavation of a circular tunnel in a bedded argillaceous rock (Opalinus Clay): short-term rock mass response and FDEM numerical analysis, *Tunn. Undergr. Space Technol.* 45 (2015) 227–248.
- [47] X.L. Li, Timodaz: a successful international cooperation project to investigate the thermal impact on the EDZ around a radioactive waste disposal in clay host rocks, *J. Rock. Mech. Geotech. Eng.* 5 (2013) 231–242.
- [48] R. McLamore, K.E. Gray, The mechanical behaviour of anisotropic sedimentary rocks, *Trans. Am. Soc. Mech. Eng. B* 89 (1967) 62–76.
- [49] B. Mahanta, T.N. Singh, P.G. Ranjith, Influence of thermal treatment on mode I fracture toughness of certain Indian rocks, *Eng. Geol.* 210 (2016) 103–114, <https://doi.org/10.1016/j.enggeo.2016.06.008>.
- [50] M. Nasserí, B. Mohanty, Fracture toughness anisotropy in granitic rocks, *Int. J. Rock. Mech. Min. Sci.* 45 (2008) 167–193, <https://doi.org/10.1016/j.ijrmms.2007.04.005>.
- [51] Y. Nara, K. Morimoto, N. Hiroyoshi, T. Yoneda, K. Kaneko, P.M. Benson, Influence of relative humidity on fracture toughness of rock: implications for subcritical crack growth, *Int. J. Solids Struct.* 49 (18) (2012) 2471–2481, <https://doi.org/10.1016/j.ijsolstr.2012.05.009>.
- [52] M. Nasserí, K. Rao, T. Ramamurthy, Anisotropic strength and deformational behavior of Himalayan schists, *Int. J. Rock. Mech. Min. Sci.* 40 (2003) 3–23, [https://doi.org/10.1016/S1365-1609\(02\)00103-X](https://doi.org/10.1016/S1365-1609(02)00103-X).
- [53] M.H. Nasserí, K.S. Rao, T. Ramamurthy, Failure mechanism in schistose rocks, *Int. J. Rock. Mech. Min. Sci.* 34 (1997) 3–4.
- [54] W.J. Phillips, N. Phillips, *An Introduction to Mineralogy for Geologists*, Wiley, New York, 1980.
- [55] B. Park, K.B. Min, Bonded-particle discrete element modeling of mechanical behavior of transversely isotropic rock, *Int. J. Rock. Mech. Min. Sci.* 76 (2015) 243–255, <https://doi.org/10.1016/j.ijrmms.2015.03.014>.
- [56] D.O. Potyondy, The bonded-particle model as a tool for rock mechanics research and application: current trends and future directions, *Geosystem. Eng.* 18 (2015) 1–28.
- [57] Potyondy, D.O. , (2012), A flat-jointed bonded-particle material for hard rock, in: Proceedings of the Forty Sixth U.S. Rock Mechanics/Geomechanics Symposium, Chicago, USA.
- [58] Potyondy, D.O. , (2017), Simulating perforation damage with a flat-jointed bonded-particle material, in: Proceedings of the Fifty First US Rock Mechanics/Geomechanics Symposium, San Francisco, California, USA.
- [59] D.O. Potyondy, P.A. Cundall, A bonded-particle model for rock, *Int. J. Rock. Mech. Min. Sci.* 41 (2004) 1329–1364.
- [60] T. Ramamurthy, G.V. Rao, J. Singh, A strength criterion for anisotropic rocks, *Proc. Int Symp. Rock. Mt. Depth* (1988) 37–44.
- [61] K.S. Rao, Strength and Deformation Behaviour of Sandstones (Ph.D. thesis), Indian Institute of Technology, Delhi, 1984.
- [62] T. Ramamurthy, Strength and modulus responses of anisotropic rocks, in: J.A. Hudson (Ed.), *Fundamentals, Comprehensive Rock Engineering*, 1, Pergamon Press, Oxford, 1993, pp. 313–329 (Fundamentals).
- [63] J. Singh, T. Ramamurthy, G. Venkatappa Rao, Strength anisotropies in rocks, *Ind. Geotech. J.* 19 (2) (1989) 147–166.
- [64] V.K. Singh, D. Singh, T.N. Singh, Prediction of strength properties of some schistose rocks from petrographic properties using artificial neural networks, *Int. J. Rock. Mech. Min. Sci.* 38 (2) (2001) 269–284.
- [65] A.B. Shemirani, H. Haeri, V. Sarfarazi, P. Ebneabbasi, M.F. Marji, Investigation of the interaction between concrete-gypsum interface and internal notch using experimental test and numerical simulation, *Mech. Based Des. Struct.* (2021) 1–24.
- [66] Seingre, G., 2005. Tunnel de base du Lötschberg-Bil an de l'excavation aux tunneliers, In: Arnould, M., Ledru, P. (Eds.), *Geoline 2005, BRGM ed.*, 23–25 May, Lyon, France.
- [67] H. Saroglou, P. Marinou, G. Tsiambaos, The anisotropic nature of selected metamorphic rocks from Greece, *J. South Afr. Inst. Min. Met.* (2004) 217–222.
- [68] V. Sarfarazi, A. Ghazvinian, W. Schubert, et al., Numerical simulation of the process of fracture of echelon rock joints, *Rock. Mech. Rock. Eng.* (2013), <https://doi.org/10.1007/s00603-013-0450-3>.
- [69] V. Sarfarazi, S. Abharian, A. Ghorbani, Physical test and PFC modelling of rock pillar failure containing two neighboring joints and one hole, *Smart Struct. Syst.* 27 (1) (2021) 123–137, <https://doi.org/10.12989/sss.2021.27.1.123>.
- [70] V. Sarfarazi, S. Abharian, N. Babanouri, H. Salari Rad, Interaction between a hole and a crack in different layouts: experimental and numerical study on concrete, *Comput. Concr.* 28 (4) (2021) 415–432, <https://doi.org/10.12989/cac.2021.28.4.415>.
- [71] V. Sarfarazi, S. Abharian, E.Z. Ghalam, Physical test and PFC2D simulation of the failure mechanism of echelon joint under uniaxial compression, *Comput. Concr.* 27 (4) (2021) 99–109, <https://doi.org/10.12989/cac.2021.27.2.099>.
- [72] J.P. Sun, Z.Y. Zhao, Effects of anisotropic permeability of fractured rock masses on underground oil storage caverns, *Tunn. Undergr. Space Technol.* 25 (2010) 629–637.
- [73] J.P. Sun, Z.Y. Zhao, Y. Zhang, Determination of three dimensional hydraulic conductivities using a combined analytical/neural network model, *Tunn. Undergr. Space Technol.* 26 (2011) 310–319.
- [74] O. Saeidi, H. Stille, R.S. Torabi, Numerical and analytical analyses of the effects of different joint and grout properties on the rock mass groutability, *Tunn. Undergr. Space Technol.* 38 (2013) 11–25.
- [75] M. Sagong, D. Park, J. Yoo, J.S. Lee, Experimental and numerical analyses of an opening in a jointed rock mass under biaxial compression, *Int. J. Rock. Mech. Min. Sci.* 48 (2011) 1055–1067.
- [76] Seeska, R., Lux, K.H., Hesser, J.B.B., 2011. Experiment: long term deformation behavior of boreholes, Mont Terri Technical Note TN 2011–04, Switzerland, Saint Ursanne.
- [77] K.E.N. Tsidzi, The influence of foliation on point load strength anisotropy of foliated rocks, *Eng. Geol.* 29 (1990) 49–58.
- [78] Y.M. Tien, P.F. Tsao, Preparation and mechanical properties of artificial transversely isotropic rock, *Int. J. Rock. Mech. Min. Sci.* 37 (2000) 1001–1012, [https://doi.org/10.1016/S1365-1609\(00\)00024-1](https://doi.org/10.1016/S1365-1609(00)00024-1).
- [79] Y.M. Tien, M.C. Kuo, A failure criterion for transversely isotropic rocks, *Int. J. Rock. Mech. Min. Sci.* 38 (3) (2001) 399–412.
- [80] A. Tavallali, A. Vervoort, Failure of layered sandstone under Brazilian test conditions: effect of micro-scale parameters on macro-scale behaviour, *Rock. Mech. Rock. Eng.* 43 (5) (2010) 641–653.
- [81] Y.M. Tien, M.C. Kuo, C. Juang, An experimental investigation of the failure mechanism of simulated transversely isotropic rocks, *Int. J. Rock. Mech. Min. Sci.* 43 (2006) 1163–1181.
- [82] Vietor, T., Li, X.L., Chen, G.J., Verstricht, J., Fisch, H., Fierz, T., 2010. Small scale in situ tests: bore-hole experiments at HADES and Mont Terri rock laboratories, Deliverable 8, TIMODAZ Project.
- [83] V. Vishal, S.P. Pradhan, T.N. Singh, Tensile strength of rock under elevated temperature, *Geotech. Geol. Eng.* 29 (2011) 1127–1133, <https://doi.org/10.1007/s10706-011-9440-y>.

- [84] A. Vervoort, K.B. Min, H. Konietzky, J.W. Cho, B. Debecker, Q.D. Dinh, T. Frühwirt, A. Tavallali, Failure of transversely isotropic rock under Brazilian test conditions, *Int. J. Rock. Mech. Min. Sci.* 70 (2014) 343–352.
- [85] J. Wang, L.Z. Xie, H.P. Xie, L. Ren, B. He, C.B. Li, Z.P. Yang, C. Gao, Effect of layer orientation on acoustic emission characteristics of anisotropic shale in Brazilian tests, *J. Nat. Gas Sci. Eng.* 36 (2016) 1120–1129.
- [86] P.T. Wang, T.H. Yang, T. Xu, M.F. Cai, C.H. Li, Numerical analysis on scale effect of elasticity, strength and failure patterns of jointed rock masses, *Geosci. J.* 20 (2016) 539–549.
- [87] P. Wasantha, P. Ranjith, Q. Zhang, T. Xu, Do joint geometrical properties influence the fracturing behaviour of jointed rock? An investigation through joint orientation, *Geomech. Geophys. Geo Energy Geo Resour.* 1 (2015) 3–14, <https://doi.org/10.1007/s40948-015-0001-3>.
- [88] T. Wang, D. Xu, D. Elsworth, W. Zhou, Distinct element modeling of strength variation in jointed rock masses under uniaxial compression, *Geomech. Geophys. Geo Energy Geo Resour.* 2 (2016) 11–24.
- [89] S.Y. Wang, S.W. Sloan, C.A. Tang, W.C. Zhu, Numerical simulation of the failure mechanism of circular tunnels in transversely isotropic rock masses, *Tunn. Undergr. Space Technol.* 32 (2012) 231–244.
- [90] X. Xia, H.B. Li, J.C. Li, B. Liu, C. Yu, A case study on rock damage prediction and control method for underground tunnels subjected to adjacent excavation blasting, *Tunn. Undergr. Space Technol.* 35 (2013) 1–7.
- [91] K. Xia, W. Yao, B. Wu, Dynamic rock tensile strengths of Laurentian granite: experimental observation and micromechanical model, *J. Rock Mech. Geotech. Eng.* 9 (2017) 116–124.
- [92] T.H. Yang, P.T. Wang, T. Xu, Q.L. Yu, P.H. Zhang, W.H. Shi, G.J. Hu, Anisotropic characteristics of fractured rock mass and a case study in Shirengou Metal Mine in China, *Tunn. Undergr. Space Technol.* 48 (2015) 129–139.
- [93] I. Yilmaz, O. Yucel, Use of the core strangle test for determining strength anisotropy of rocks, *Int. J. Rock. Mech. Min. Sci.* 66 (2014) 57–63.
- [94] T. Yin, X. Li, K. Xia, S. Huang, Effect of thermal treatment on the dynamic fracture toughness of Laurentian granite, *Rock. Mech. Rock. Eng.* 45 (2012) 1087–1094, <https://doi.org/10.1007/s00603-012-0240-3>.
- [95] C. Yu, S.C. Deng, H.B. Li, J.C. Li, X. Xia, The anisotropic seepage analysis of watersealed underground oil storage caverns, *Tunn. Undergr. Space Technol.* 38 (2013) 26–37.
- [96] R. Yuan, B. Shen, Numerical modelling of the contact condition of a Brazilian disk test and its influence on the tensile strength of rock, *Int. J. Rock Mech. Min. Sci.* 93 (2017) 54–65.
- [97] S.W. Zhang, K.J. Shou, X.F. Xian, J.P. Zhou, G.J. Liu, Fractal characteristics and acoustic emission of anisotropic shale in Brazilian tests, *Tunn. Undergr. Space Technol.* 71 (2018) 298–308.
- [98] Q. Zhang, J. Zhao, Effect of loading rate on fracture toughness and failure micromechanisms in marble, *Eng. Fract. Mech.* 102 (2013) 288–309, <https://doi.org/10.1016/j.engfracmech.2013.02.009>.
- [99] X.P. Zhang, L.N.Y. Wong, S.J. Wang, G.Y. Han, Engineering properties of quartz mica schist, *Eng. Geol.* 121 (2011) 135–149.